STATISTICS, OPTIMIZATION AND INFORMATION COMPUTING
Stat., Optim. Inf. Comput., Vol. **16**, August 2026, pp 1379–1393.
Published online in International Academic Press (www.IAPress.org)

Dual Reciprocity Boundary Element Method-based analysis of infiltration in heterogeneous soils under different irrigation channel types

Millatuz Zahroh*, Maq Rifatur Rosiyanti, Moh. Hasan

Department of Mathematics, University of Jember, Indonesia

Abstract The research discussed analysis of infiltration in heterogeneous soils under different irrigation channel types. The heterogenous soils consist of layer 1 is silt loam (SL) and layer 2 is pima clay loam (PCL). Irrigation channel types that discussed consist of trapezoidal, rectangular, semi-circular, triangular, impermeable based of trapezoidal , and impermeable based of rectangular channel. The problem is governed as Richards' equation converted into a modified Helmholtz equation to serve as a mathematical model. This model is then solved numerically using the Dual Reciprocity Boundary Element Method (DRBEM). The resulting numerical solution is the suction potential in each type of irrigation channels. The area below of the channels with the highest suction potential value are the irrigation channels without impermeable. In irrigation channels with impermeable based, the area below of the channels has a low suction potential value. The solution also indicate that there are jumps of suction potential value from layer 1 to layer 2. The order of highest to lowest suction potential values obtained from the solution are triangular, rectangular, semi-circular, impermeable based of trapezoidal, and impermeable based of rectangular channel.

Keywords channel variations, infiltration, heterogenous soils, DRBEM

DOI: 10.19139/soic-2310-5070-4210

1. Introduction

Water is an essential natural resource that plays a significant role in the agricultural and plantation sectors, amounting to 70%. Water in the agriculture and plantation sector is used for irrigation, which is very important for providing nutrition and plant survival [1]. Efficient water management in agricultural systems is critically dependent on understanding the infiltration behavior of soils under various irrigation conditions [2, 3]. Infiltration, the process by which water penetrates the soil surface and moves through the subsurface layers, is significantly influenced by both soil heterogeneity and the structural design of irrigation channels. As the global demand for water-efficient agriculture intensifies, especially in regions facing water scarcity, a detailed understanding of the infiltration process becomes increasingly essential [4, 5].

Infiltration is influenced by the condition of the soil surface in the structural design of irrigation channels. The general types are flat, rectangular, triangular, trapezoidal, and semi-circular channels [6, 7]. Infiltration is also influenced by soil texture and soil structure because each type of soil has a different absorption rate. Soil structure generally consists of several types of soil that are called heterogeneous soil [8, 9]. Heterogeneous soils, characterized by variations in texture, porosity, and hydraulic conductivity, present complex challenges for predicting water movement.

Traditional numerical approaches for modeling water infiltration, such as the Finite Element Method (FEM) [10, 11] and the Finite Difference Method (FDM) [12], have been widely used to solve flow problems in porous media. Although these methods provide reliable approximations, they require domain discretization and extensive

*Correspondence to: Millatuz Zahroh (Email: millatuz@unej.ac.id). Department of Mathematics, University of Jember. Kalimatan Street 37, Jember, East Java, Indonesia (68121).

ISSN 2310-5070 (online) ISSN 2311-004X (print)

meshing, which may become computationally expensive when dealing with heterogeneous soils, layered domains, or complex irrigation-channel geometries. Analytical solutions have also been developed for specific infiltration scenarios [15, 16]; however, their applicability is often restricted by simplifying assumptions regarding soil properties and boundary configurations. To overcome these limitations, boundary-based and meshless techniques have attracted considerable attention. In particular, the Boundary Element Method (BEM) and the Dual Reciprocity Boundary Element Method (DRBEM) have proven effective for solving infiltration problems because they reduce the dimensionality of the problem and transform domain integrals into equivalent boundary formulations [13, 14, 21]. Recent developments have also demonstrated the potential of meshless approaches for modeling infiltration in heterogeneous soils [23].

Several studies have investigated infiltration behavior in heterogeneous soils using analytical and numerical methods. For example, Zumr and Jeř'abek [22] examined the influence of soil heterogeneity on infiltration patterns, showing that abrupt changes in soil properties significantly affect water movement. Similarly, previous studies have shown that infiltration behavior in layered soils may exhibit discontinuities in suction potential and infiltration rate due to variations in hydraulic conductivity and soil texture. Despite these advances, most existing investigations have focused either on soil heterogeneity or on channel geometry separately. Comprehensive studies that simultaneously evaluate heterogeneous soils and multiple irrigation-channel geometries remain limited.

The influence of channel geometry on infiltration efficiency is still debated. Yilmaz and Akin [17] reported that semi-circular channels promote a more uniform moisture distribution owing to their curved wetted perimeter, whereas Al-Janabi [18] concluded that trapezoidal channels enhance deeper water penetration in layered soils. These differing conclusions suggest that the effectiveness of a particular channel geometry depends strongly on subsurface conditions and soil heterogeneity. Therefore, a systematic comparison of different channel shapes under identical heterogeneous-soil conditions is necessary to clarify how channel geometry affects suction potential distribution and infiltration performance.

The present study builds upon the authors' previous work. Solekhudin et al.[21] and Nurhasanah et al. [27] applied a boundary element formulation to analyze infiltration of different types channel in homogeneous soils, while Zahroh et al. [9] investigated infiltration behavior in layered soils using DRBEM. Consequently, the novelty of this study lies in the application of DRBEM to systematically evaluate the combined effects of soil heterogeneity, irrigation-channel geometry, and impermeable-layer conditions on infiltration behavior. The results provide new insights into the relationship between channel shape and infiltration efficiency, thereby contributing to the design of more effective irrigation systems.

This study aims to research the use of DRBEM to solve the effect of irrigation channel types on heterogeneous soil infiltration. The types are trapezoidal, rectangular, semi-circular, triangular, trapezoidal with impermeable, and rectangular with impermeable channels. This heterogeneous soil are consist of silt loam, layer 1, and pima clay loam, layer 2. By computing suction potential distributions across soil layers and channel profiles, this work seeks to determine which channel types most effectively promote infiltration under given soil conditions. The results are expected to offer valuable insights for optimizing irrigation design in agricultural engineering, particularly in regions with complex soil structures.

2. Basic Equation and Formulation

The research discussed six types of irrigation channels, namely triangular, rectangular, semi-circular, impermeable based on trapezoidal, and impermeable based on rectangular channels. The irrigation channel is very long, so it can be considered as two dimensional problem[10]. The research also assume that infiltration independ on time and infiltration occurs only on the channel surface. Then, the absorption of water by the plant is neglected. This problem is illustrated in Figure 1

The area we are analyzing is a large, two-dimensional rectangle. It stretches from $X = 0$ to a distance $X = L + D$ to the side of the channel, and from the ground level ($Z = 0$) down to an indefinite depth ($Z \geq 0$). The surface length of the irrigation channel is assumed to be $2L$. Within the mathematical model, the physical size of the irrigation channel is not arbitrary; its width and depth are precisely determined by the key length parameter

L using the formulas $2L/\pi$ and $3L/(2\pi)$, respectively. The initial incoming flux is $v_0 = 0.75 \times K_0$. The incoming water flow is only present on the surface of the channel, meaning that the normal flux at other boundaries is zero. At infinite depth, it is assumed that the *potential* for water to move (due to soil suction) drops to nothing because the deep soil is dry. $\frac{\partial X}{\partial \Theta} \to 0$ There is no significant change in this potential from left to right at great depth. This implies no appreciable horizontal water flow at that level $\frac{\partial Z}{\partial \Theta} \to 0$. There is no significant change in this potential from top to bottom at great depth. This implies no appreciable vertical water flow moving downward as $Z \to \infty$

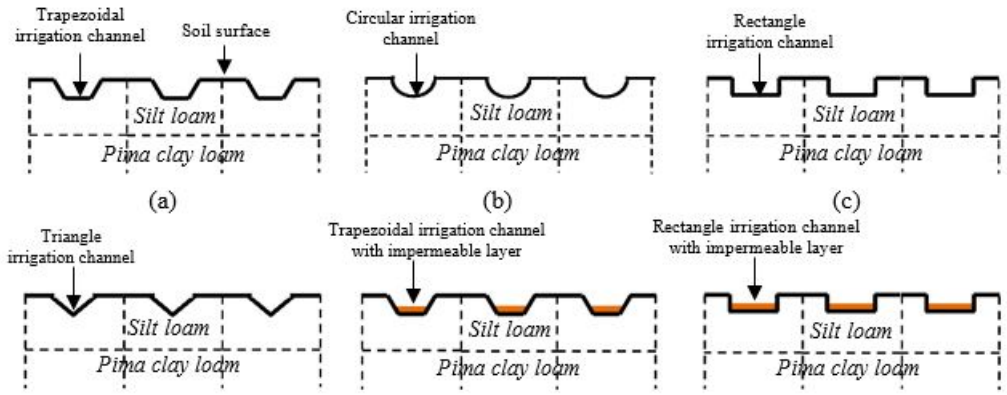

Figure 1. Irrigation channels types in heterogeneous soils **(a)** Trapezoidal channel, **(b)** Semi-circular channel, **(c)** Rectangular channel, **(d)** triangular channel, **(e)** Trapezoidal channel with impermeable, **(f)** Rectangular channel with impermeable

The mathematical model that is often used in infiltration problems is commonly known as the **Richards Equation**. The equation independ on time is:

$$\frac{\partial}{\partial X}\left[K(\psi)\frac{\partial \psi}{\partial X}\right] + \frac{\partial}{\partial Z}\left[K(\psi)\left(\frac{\partial \psi}{\partial Z} - 1\right)\right] = 0 \tag{1}$$

where $K(\psi)$ is the unsaturated hydraulic conductivity and ψ is the suction potential, x is the horizontal direction, z is the vertical direction (positive downward). However, The original time-independent Richards Equation is a non-linear partial differential equation that is difficult to solve. To simplify it, the required transformations are as follows:

1. Kirchhoff Transformation and Exponential Relationship

$$\Theta = \int_{-\infty}^{\psi} K(q)\, dq \tag{2}$$

$$K(\psi) = K_0 e^{\alpha\psi}, \quad \alpha > 0 \tag{3}$$

where Θ is the *Matric Flux Potential (MFP)*, α is the constant soil parameter, K_0 is the hydraulic conductivity under saturated soil conditions, and $K(\psi)$ is the hydraulic conductivity under unsaturated conditions. The MFP describes the distribution of water spread in the soil. This research uses two different soil layers, each having different parameter values for soil proportion (α) and hydraulic conductivity in saturated soil (K_0). Therefore, an average value of α and K_0 is required, which is denoted by α^* and K_0^*. From equations 2 and 3, we obtain:

$$\alpha^*\Theta = K_0^* e^{\alpha^*\psi} \tag{4}$$

Equations 2 and 4 can be used to convert equation 1 into the following form:

$$\frac{\partial^2\Theta}{\partial X^2}+\frac{\partial^2\Theta}{\partial Z^2}-\alpha^*\frac{\partial\Theta}{\partial Z}=0 \tag{5}$$

with the outward normal flux $\mathbf{n}=(n_1,n_2)$ given by:

$$F=-\frac{\partial\Theta}{\partial X}n_1+\left(\alpha^*\Theta-\frac{\partial\Theta}{\partial Z}\right)n_2 \tag{6}$$

2. Transformation with Dimensionless Variables

$$\begin{aligned}&x=\frac{\alpha^*}{2}X,\quad z=\frac{\alpha^*}{2}Z,\quad u=\frac{2\pi}{v_0\alpha^*L}U,\quad v=\frac{2\pi}{v_0\alpha^*L}V,\\&f=\frac{2\pi}{v_0\alpha^*L}F,\quad \Phi=\frac{\pi\Theta}{v_0L}\end{aligned} \tag{7}$$

where v_0 is the initial flux, L is half the length of the irrigation channel, and Φ is the MFP in dimensionless form.
Equation 5 is tranformed by Equation 7 we have

$$\begin{aligned}&\frac{\partial^2\Theta}{\partial X^2}+\frac{\partial^2\Theta}{\partial Z^2}-\alpha^*\frac{\partial\Theta}{\partial Z}=0\\&\frac{v_0\alpha^{*2}L}{4\pi}\frac{\partial^2\Phi}{\partial x^2}+\frac{v_0\alpha^{*2}L}{4\pi}\frac{\partial^2\Phi}{\partial z^2}-\alpha^*\frac{\alpha^*v_0L}{2\pi}\frac{\partial\Phi}{\partial z}=0\\&\frac{\partial^2\Phi}{\partial x^2}+\frac{\partial^2\Phi}{\partial z^2}=2\frac{\partial\Phi}{\partial z}\end{aligned} \tag{8}$$

with the normal flux given as

$$f=-\frac{\partial\Phi}{\partial x}n_1+\left(2\Phi-\frac{\partial\Phi}{\partial z}\right)n_2 \tag{9}$$

3. Exponential Transformation
This transformation assumes:

$$\Phi=\varphi e^z,\quad z\neq 0 \tag{10}$$

using Equation 10, Equation 8 is transformed in

$$\begin{aligned}&e^z\frac{\partial^2\varphi}{\partial x^2}+e^z\left(\frac{\partial^2\varphi}{\partial z^2}+2\frac{\partial\varphi}{\partial z}+\varphi\right)-2e^z\left(\frac{\partial\varphi}{\partial z}+\varphi\right)=0\\&e^z\frac{\partial^2\varphi}{\partial x^2}+e^z\frac{\partial^2\varphi}{\partial z^2}-e^z\varphi=0\\&\frac{\partial^2\varphi}{\partial x^2}+\frac{\partial^2\varphi}{\partial z^2}=\varphi\end{aligned} \tag{11}$$

Finally, the result of transforming Richards' Equation 3 is the following Modified Helmholtz Equation:

$$\frac{\partial^2\varphi}{\partial x^2}+\frac{\partial^2\varphi}{\partial z^2}=\varphi \tag{12}$$

where ϕ is the solution to the Modified Helmholtz Equation in terms of MFP. Equation 12 is supplemented by the dimensionless flux:

$$f=-e^z\left(\frac{\partial\varphi}{\partial n}-\varphi n_2\right) \tag{13}$$

Equation 12 is the equation whose solution is sought so that the solution can be used to determine the suction potential (ψ) for any irrigation channel geometry.
The φ value is used to obtain the suction potential values for two layers of heterogeneous soil, ranging from fine to coarse soil textures. The suction potential value can be obtained using:

$$\psi = \frac{1}{\alpha_i} \ln \left(\frac{v_0 L \alpha_i \varphi e^z}{\pi K_{0_i}} \right) \tag{14}$$

where $i = 1, 2$

By utilizing the transformation as in the previous paragraph and Equation (3)-(13), the boundary conditions in dimensionless for the irrigation channel models, both without and with an impermeable layer ($L = 50$), are prescribed on the boundaries $z = 0$ and $z = 4$ [20]. The surface boundary is given by

1. Boundary Conditions for Irrigation Channel without Impermeable Layer

$$\frac{\partial \varphi}{\partial n} = \varphi n_2 + \frac{2\pi}{50\alpha} e^{-z}, \quad \text{on the channel surface} \tag{15}$$

$$\frac{\partial \varphi}{\partial n} = -\varphi, \quad \text{for } \frac{50\alpha}{\pi} \le x \le \frac{\alpha}{2}(50 + D),\ z = 0 \text{ and } 0 \le x \le \frac{\alpha}{2}(50 + D),\ z = 4 \tag{16}$$

$$\frac{\partial \varphi}{\partial n} = 0, \quad \text{for } x = \frac{\alpha}{2}(50 + D),\ z \ge 0 \text{ and } x = 0,\ z \ge \frac{150\alpha}{4\pi} \tag{17}$$

2. Boundary Conditions for Irrigation Channel with Impermeable Layer

$$\frac{\partial \varphi}{\partial n} = \varphi n_2 + \frac{2\pi}{50\alpha} e^{-z}, \quad \text{on the permeable channel surface} \tag{18}$$

$$\frac{\partial \varphi}{\partial n} = \varphi n_2, \quad \text{on the impermeable channel surface} \tag{19}$$

$$\frac{\partial \varphi}{\partial n} = -\varphi, \quad \text{for } \frac{50\alpha}{\pi} \le x \le \frac{\alpha}{2}(50 + D),\ z = 0 \text{ and } 0 \le x \le \frac{\alpha}{2}(50 + D),\ z = 4 \tag{20}$$

$$\frac{\partial \varphi}{\partial n} = 0, \quad \text{for } x = \frac{\alpha}{2}(50 + D),\ z \ge 0 \text{ and } x = 0,\ z \ge \frac{150\alpha}{4\pi} \tag{21}$$

3. DRBEM for Infiltration in Irrigation Channel

This section explains how to solve the Modified Helmholtz 12 for an irrigation channel that lacks an impermeable layer. The solution is achieved by applying the Dual Reciprocity Boundary Element Method (DRBEM) procedure, using the specific boundary conditions outlined in 15-17.

The boundary value problem for the irrigation channel is solved using the DRBEM as formulated in 22.

$$\lambda(\xi, \eta)\varphi(\xi, \eta) = \int_C \left[\varphi(x, z) \frac{\partial \Upsilon(x, z; \xi, \eta)}{\partial n} - \Upsilon(x, z; \xi, \eta) \frac{\partial \varphi(x, z)}{\partial n} \right] ds + \iint_R \Upsilon(x, z; \xi, \eta)\varphi(x, z), dx, dz \tag{22}$$

where

$$\lambda(\xi,\eta)=\begin{cases}0, & \text{if } (\xi,\eta)\notin R\cup C\\ \frac{1}{2}, & \text{if } (\xi,\eta) \text{ is on the smooth part of } C\\ 1, & \text{if } (\xi,\eta)\in R\end{cases} \tag{23}$$

and Υ is fundamental laplace solution Then, we use the boundary conditions 18-21 for Irrigation Channel with Impermeable Layer resulting in:

$$\begin{aligned}\lambda(\xi,\eta)\varphi(\xi,\eta)=&\int_{C_1}\left[\varphi(x,z)\frac{\partial\Upsilon(x,z;\xi,\eta)}{\partial n}-\Upsilon(x,z;\xi,\eta)\left(\frac{2\pi}{\alpha L}e^{-z}+\varphi n_2\right)\right]ds(x,z)\\&+\int_{C_2\cup C_5}\varphi(x,z)\left[\frac{\partial\Upsilon(x,z;\xi,\eta)}{\partial n}+\Upsilon(x,z;\xi,\eta)\right]ds(x,z)\\&+\int_{C_3\cup C_4}\varphi(x,z)\frac{\partial\Upsilon(x,z;\xi,\eta)}{\partial n}ds(x,z)+\iint_R\Upsilon(x,z;\xi,\eta)\varphi(x,z)dxdz\end{aligned}$$

Using DRBEM Procedure, we have

$$\begin{aligned}\lambda(a^{(n)},b^{(n)})\varphi^{(n)}=&\sum_{k=1}^{N}\varphi^{(k)}\left[\Upsilon_2^{(k)}(a^{(n)},b^{(n)})-v^{(k)}\Upsilon_1^{(k)}(a^{(n)},b^{(n)})\right]\\&-\sum_{k=1}^{N}fl^{(k)}e^{-b^{(k)}}\Upsilon_1^{(k)}(a^{(n)},b^{(n)})+\sum_{j=1}^{N+M}\mu^{(n,j)}\varphi^{(j)}\end{aligned} \tag{24}$$

for,

$$v^{(k)}=\begin{cases}0, & C^{(k)}\in C_3\cup C_4\\ 1, & C^{(k)}\in C_2\cup C_5\\ n_2, & C^{(k)}\in C_1\end{cases}$$

where

$$\begin{aligned}\Upsilon_1^{(k)}=&\frac{1}{4\pi}\int_{C^{(k)}}\ln\left[(x-a)^2+(y-b)^2\right]ds\\ \Upsilon_2^{(k)}=&\frac{1}{4\pi}\int_{C^{(k)}}\frac{\partial}{\partial n}\left[\ln\left[(x-a)^2+(y-b)^2\right]\right]ds\end{aligned} \tag{25}$$

and

$$\sum_{j=1}^{N+M}\mu^{(n,j)}=\sum_{j=1}^{N+M}\left[\sum_{m=1}^{N+M}\omega(a^{(j)},b^{(j)};a^{(m)},b^{(m)})\Psi(a^{(n)},b^{(n)};a^{(m)},b^{(m)})\right]$$

where $\varphi^{(n)}$ is the value of φ evaluated at $(a^{(n)},b^{(n)})$, $fl^{(k)}$ is the inward flux at the collocation point $(a^{(k)},b^{(k)})$ and n_2 is the normal vector along the Z-axis.

The terms containing $\varphi^{(k)}$, for $k = 1, 2, 3, ...$ in Equation 24 and the remaining terms are on the right-hand side, so we have

$$\begin{aligned}
&\sum_{k=1}^{N}\left[\Upsilon_2^{(k)}(a^{(n)},b^{(n)}) - v^{(k)}\Upsilon_1^{(k)}(a^{(n)},b^{(n)})\right]\varphi^{(k)} \\
&+ \sum_{j=1}^{N+M}\mu^{(n,j)}\varphi^{(j)} - \lambda(a^{(n)},b^{(n)})\varphi^{(n)} \\
&= \sum_{k=1}^{N} fl^{(k)}e^{-b^{(k)}}\Upsilon_1^{(k)}(a^{(n)},b^{(n)})
\end{aligned} \tag{26}$$

Equation 26 can be rewritten as the following system

$$\sum_{k=1}^{N+M} A_{nk}\varphi^{(k)} = b_{nk} \tag{4.22}$$

where

$$b_{nk} = \sum_{k=1}^{N} fl^{(k)}e^{-b^{(k)}}\Upsilon_1^{(k)}(a^{(n)},b^{(n)}) \tag{4.23}$$

for

$$\begin{aligned}
A_{nk} =& \Upsilon_2^{(k)}(a^{(n)},b^{(n)}) - v^{(k)}\Upsilon_1^{(k)}(a^{(n)},b^{(n)}) + \mu(a^{(n)},b^{(n)};a^{(k)},b^{(k)}) - \frac{1}{2}\epsilon^{(nk)}, \\
&\text{for } k = 1, 2, \ldots, N \\
A_{nk} =& \mu(a^{(n)},b^{(n)};a^{(k)},b^{(k)}) - \epsilon^{(nk)}, \text{ for } k = N+1, \ldots, N+M
\end{aligned} \tag{27}$$

with

$$\epsilon^{(nk)} = \begin{cases} 0, & k \neq n \\ 1, & k = n \end{cases}$$

In the Dual Reciprocity Boundary Element Method (DRBEM), the nonhomogeneous term of the governing equation is approximated using radial basis functions (RBFs). In this study, a polynomial radial basis function is employed due to its simplicity, numerical stability, and successful application in previous DRBEM formulations for infiltration and groundwater-flow problems [25].

The boundary integral equations were discretized using boundary nodes and interior collocation points. The number of boundary nodes (N) was determined according to the geometric complexity and perimeter of each irrigation-channel configuration, whereas the number of interior nodes (M) was selected to adequately represent the spatial variation of suction potential within the heterogeneous soil domain. Consequently, the values of N and M vary among the trapezoidal, rectangular, semi-circular, and triangular channel geometries because each geometry possesses a different boundary configuration and domain discretization requirement.

4. Experimental results

This research uses two different soil layers with different parameter values for soil proportion, α, and hydraulic conductivity in saturated soil, K_0. Therefore, an average value of α is required which is symbolized by α^*. For example, the value α_1 is a parameter for the proportion of soil layer 1, silt loam (SL), and α_2 is a parameter for the

proportion of soil layer 2, pima clay loam (PCL), then the value of α^* is

$$\alpha^* = \frac{\alpha_1 + \alpha_2}{2} = \frac{1{,}39 \times 10^{-2} + 1{,}40 \times 10^{-2}}{2} = \frac{2{,}79 \times 10^{-2}}{2} = 1{,}395 \times 10^{-2} \tag{28}$$

The solution using DRBEM uses discretization for trapezoidal channel of $N = 197$ and $M = 619$, and rectangular channel of $N = 197$ and $M = 617$. Discretization for semicircular channel is $N = 196$ and $M = 619$, and triangular channel are $N = 193$ and $M = 623$. Below are given the suction potential values of each type of irrigation channel without impermeable at several points.

4.1. Suction Potential for Irrigation Channels without Impermeable Condition

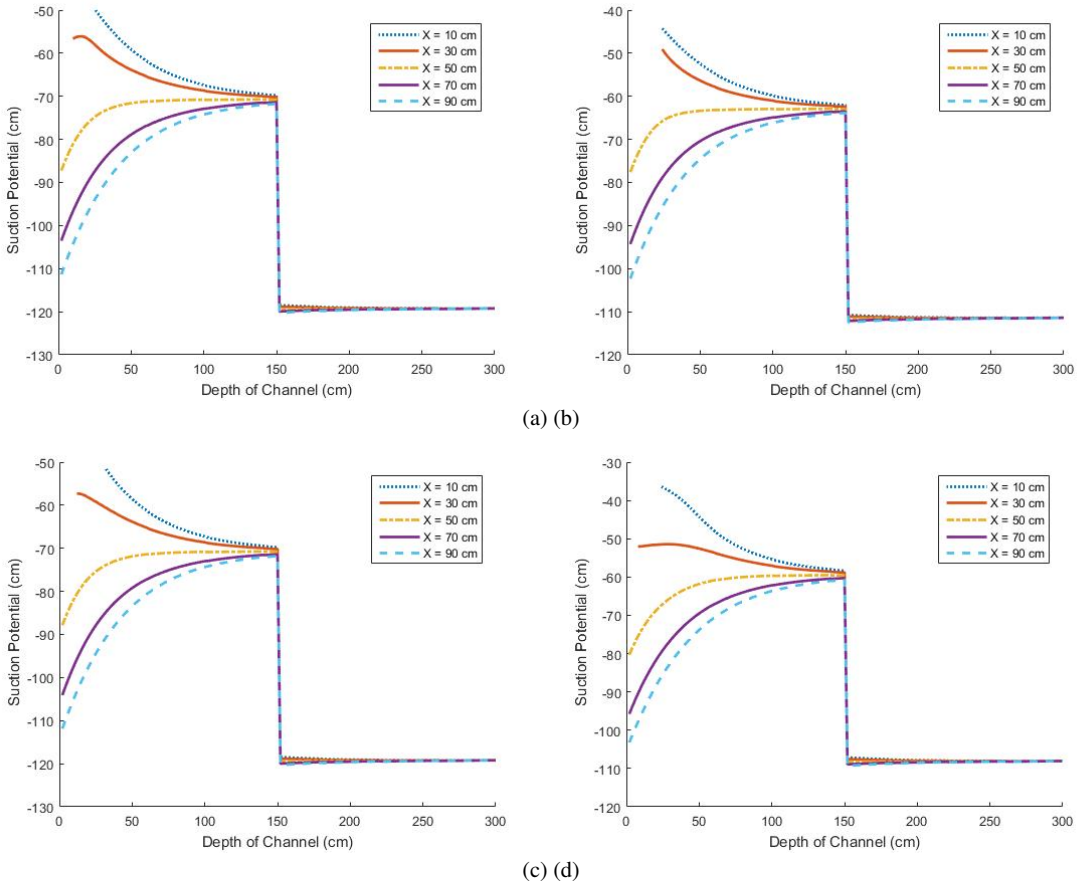

Figure 2. Suction Potential Graph for Irrigation Channels without Impermeable **(a)** Trapezoidal, **(b)** Rectangular, **(c)** Triangular, **(d)** Semi-Circular

Figure 2 illustrates the suction potential (ψ) values in irrigation channels without impermeable layers along the selected value of X. As observed in the graph, the trapezoidal, rectangular, triangular, and semi-circular channels exhibit similar patterns in the distribution of suction potential. so the results of the analysis carried out can be applied to these four channels. The highest suction potential value is at X equal 10 cm, then 30 cm and gradually decreases, reaching the lowest value at X equal 90 cm. Based on this, it can be seen that the closer the point is to the surface of the channel along X, the greater the suction potential value. The value of ψ at X equal 10 cm and X equal 30 cm decreases as the depth of the channel increases towards the point of convergence. Conversely, at X equal 50 cm, X equal 70 cm, and X equal 90 cm, the ψ values tend to increase toward their convergence point. A

decreasing suction potential indicates that less water is absorbed as depth increases, and this trend reverses when suction potential increases.

Table 1. Suction Potential Value in Irrigation Channels without Impermeable

Type of Channel	**Soil**	**(X, Z) (cm,cm)**	**Suction Potential (cm)**	**ψ Change (%)**
Trapezoidal	SL	(10, 40)	-55.96581114	-24.14%
		(10, 140)	-69.47611753	
		(90, 40)	-86.69878940	+16.99%
		(90, 140)	-71.96930023	
	PCL	(10, 175)	-118.80563685	-0.38%
		(10, 275)	-119.25655835	
		(90, 175)	119.86001206	+0.43%
		(90, 275)	-119.34314410	
Rectangular	SL	(10, 40)	-49.74420466	-24.14%
		(10, 140)	-61.75372301	
		(90, 40)	-78.01482102	+17.89%
		(90, 140)	-64.05617934	
	PCL	(10, 175)	-111.07363076	-0.33%
		(10, 275)	-111.43838623	
		(90, 175)	-112.04655087	+0.47%
		(90, 275)	-111.52027152	
Semi-circular	SL	(10, 40)	-55.09659028	-26.04%
		(10, 140)	-69.44455753	
		(90, 40)	-87.08895153	+17.30%
		(90, 140)	-72.02433416	
	PCL	(10, 175)	-118.79272448	-0.36%
		(10, 275)	-119.22511833	
		(90, 175)	-119.88225202	+0.47%
		(90, 275)	-119.31513873	
Triangular	SL	(10, 40)	-40.49396508	-43.15%
		(10, 140)	-57.96826480	
		(90, 40)	-77.72495622	+21.59%
		(90, 140)	-61.00353584	
	PCL	(10, 175)	-107.53176581	-0.5%
		(10, 275)	-108.06481160	
		(90, 175)	-108.81543441	+0.59%
		(90, 275)	-108.17570169	

Table 1 shows the suction potential values generated in the irrigation channel without an impermeable layer at X equal 10, which is a point near the channel, and X equal 90, which is located far from the channel surface. The quantity ψ Change (%) represents the percentage change in suction potential between two depths at the same horizontal location (X) within the same soil layer. For Layer 1 (SL), the comparison is made between $Z = 40$ cm and $Z = 140$ cm, whereas for Layer 2 (PCL), the comparison is made between $Z = 175$ cm and $Z = 275$ cm.

Based on Table 1, it can be observed that the suction potential values in the area close to or directly beneath the channel decrease as the channel depth increases for each irrigation channel. The decrease in Layer 1, which is silt loam, is greater than the decrease in Layer 2, which is pima clay loam. In the area far from the channel, the suction potential values increase as the depth increases. The increase in Layer 1 is greater than the increase in Layer 2. The decrease or increase in Layer 2 becomes smaller until, at a certain depth, there is no longer any decrease or increase in the suction potential value, indicating that it has reached its convergence point.

Based on Figure 2 and Table 1, a distinct jump in the suction potential is observed at the interface between Layer 1 and Layer 2, located at approximately (Z=150) cm within the 300 cm soil profile. This discontinuity is not merely a consequence of differences in soil texture; rather, it arises from the abrupt change in the hydraulic properties of the two soil layers, particularly the soil-water retention parameter (α) and the saturated hydraulic conductivity (K_0).

The parameter α governs the relationship between soil water content and matric suction, while K_0 controls the ease with which water can move through the soil. At the interface, the transition from silt loam (Layer 1) to pima clay loam (Layer 2) results in a sudden change in both water-retention characteristics and hydraulic conductivity. Consequently, the suction potential required to maintain water flow across the interface differs between the two layers, producing the observed jump in the potential profile.

Physically, this phenomenon reflects the adjustment of the hydraulic gradient as water moves from a relatively more permeable medium to a less permeable one. The lower hydraulic conductivity of Layer 2 restricts downward water movement, causing water to accumulate above the interface and creating a sharper variation in suction potential. As a result, Layer 1 exhibits higher suction-potential values than Layer 2. The magnitude of the jump therefore represents the hydraulic contrast between the two soil layers and indicates the resistance encountered by infiltrating water at the interface. Such behavior is characteristic of layered heterogeneous soils, where discontinuities in hydraulic properties lead to non-uniform distributions of matric potential and infiltration flux.

The discontinuity in suction potential is consistent with the continuity of water flux across the interface, where changes in K_0 must be compensated by corresponding changes in the hydraulic gradient according to Darcy's law.

4.2. Suction Potential for Irrigation Channels with Impermeable Condition

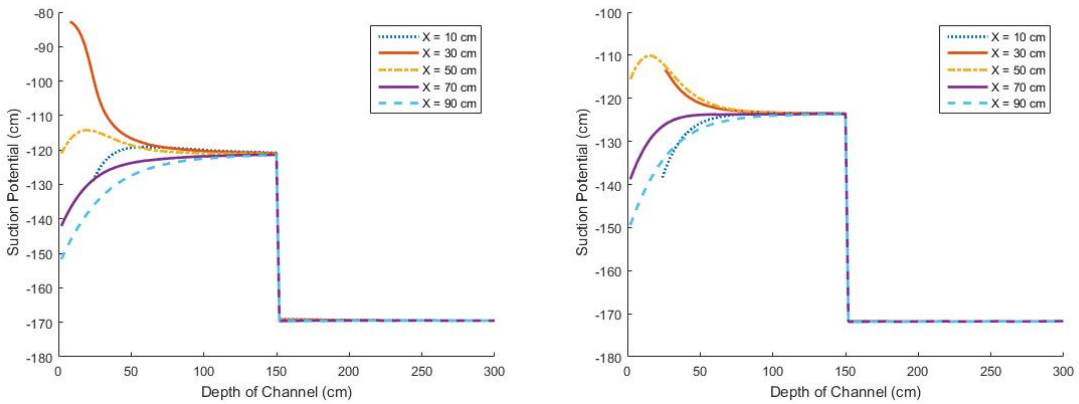

(a) (b)

Figure 3. Suction Potential Graph for Irrigation Channels with Impermeable **(a)** Trapezoidal with Impermeable, **(b)** Rectangular with Impermeable

Figure 3 shows the suction potential (ψ) values in trapezoidal and rectangular channels with an impermeable layer along the selected value of X. As observed in Figure 3(a), the ψ values in the trapezoidal channel with an impermeable layer increase with depth toward the convergence point, except at X equal 30 cm and X equal 50 cm, where a decrease is observed. In Layer 1, the highest suction potential is found at X equal 30 cm, while the lowest is at X equal 90 cm.

Similarly, in the rectangular channel with an impermeable layer, the ψ values decrease at X equal 30 cm and $X = 50$ cm. Based on Figure 3(b), in Layer 1, the highest suction potential is located at X equal 50 cm, while the lowest is at X equal 90 cm. The suction potential at X equal 90 cm has the lowest value, indicating that the farther the point is from the channel surface, the less water is absorbed by the soil.

The distribution of suction potential in irrigation channels with an impermeable layer differs significantly from that observed in channels without an impermeable layer because the impermeable boundary alters the flow pathways available for infiltrating water. In the absence of an impermeable layer, water can move downward through the soil profile under the combined effects of gravity and matric forces, resulting in a broader distribution of moisture and a relatively gradual variation in suction potential. In contrast, the impermeable layer restricts vertical flow and forces water to redistribute laterally within the soil domain.

As shown in Figure 3, the highest suction potential (least negative ψ) occurs near the water-absorbing boundary, where the soil remains relatively wet due to continuous infiltration. As the distance from the infiltration boundary increases, the suction potential becomes more negative, indicating a decrease in water content and an increase in matric suction. Therefore, the observed variation in ψ reflects the redistribution of soil moisture rather than simply the amount of water absorbed.

The presence of the impermeable layer intensifies this effect by preventing downward percolation. Water accumulates above the impermeable boundary and is redirected laterally, producing steeper suction-potential gradients within the soil profile. Consequently, the more negative suction-potential values observed in the impermeable-layer case indicate stronger matric forces associated with the restricted movement of water rather than reduced infiltration. Physically, these results suggest that the impermeable layer modifies the infiltration pattern by limiting vertical drainage, increasing moisture retention above the barrier, and altering the spatial distribution of suction potential throughout the heterogeneous soil system.

Table 2. Suction potential values in irrigation channels with an impermeable layer

Type of Channel	**Soil**	**(X, Z) (cm,cm)**	**Suction Potential (cm)**	**ψ Change (%)**
Trapezoidal with impermeable	SL	(10, 40)	-120.57193374	+0.14%
		(10, 120)	-120.40299958	
		(90, 40)	-129.93732664	+6.16%
		(90, 120)	-121.92826583	
	PCL	(10, 175)	-169.19306844	-0.18%
		(10, 275)	-169.50534893	
		(90, 175)	-169.58526311	+0.0278%
		(90, 275)	-169.53820098	
Rectangular with impermeable	SL	(10, 40)	-128.33204649	+3.81%
		(10, 120)	-123.44393763	
		(90, 40)	-129.05783395	+4.07%
		(90, 120)	-123.80882656	
	PCL	(10, 175)	-171.73537509	-0.0277%
		(10, 275)	-171.78291414	
		(90, 175)	-171.83093231	+0.0242%
		(90, 275)	-171.78938468	

Table 2 shows the suction potential values generated in the irrigation channel with an impermeable layer. The values are reported at two horizontal positions, namely $X = 10$ cm, and $X = 90$ cm. For each horizontal location, suction potential is evaluated at two depths within the same soil layer. The column "ψ Change (%)" denotes the percentage change in suction potential between these two depths while keeping the horizontal coordinate X constant.

For Layer 1 (silt loam), the suction potential generally becomes less negative with increasing depth, resulting in positive values of ψ Change. This behavior is attributed to the presence of the impermeable layer, which restricts downward percolation and promotes the redistribution of water within the upper layer. Consequently, moisture is retained within Layer 1, reducing the magnitude of matric suction at greater depths.

In contrast, Layer 2 (pima clay loam) exhibits only minor variations in suction potential between the two depths, as indicated by the small values of ψ Change. This suggests that the suction-potential distribution within the lower

layer is relatively uniform. The limited variation can be attributed to the low hydraulic conductivity of the clay-rich soil and the influence of the impermeable boundary, which together reduce vertical changes in water movement within the layer.

In the area far from the channel, the suction potential values increase as the depth increases. The increase in Layer 1 is greater than that in Layer 2. The increase in Layer 2 becomes progressively smaller until, at a certain depth, there is no further increase in suction potential, indicating that it has reached the convergence point.

4.3. Suction Potential for Each Type of Irrigation Channel

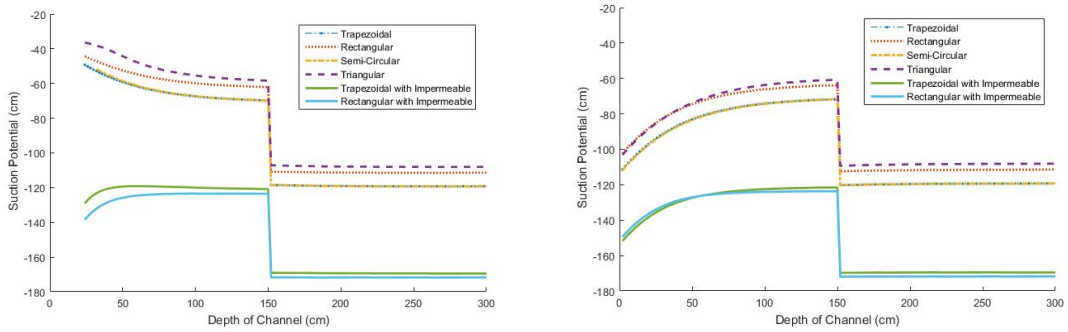

(a) (b)

Figure 4. Suction Potential for Each Type of Irrigation Channel in **(a)** $X = 10$, **(b)** $X = 90$

The variation of soil suction potential with respect to channel depth for various irrigation channel geometries and lining conditions is illustrated in Figure 4. Suction potential serves as a direct indicator of soil moisture dynamics, where less negative values signify higher moisture content due to water seepage, and highly negative values indicate drier soil conditions resulting from successful seepage mitigation. A holistic evaluation of the figures reveals that the presence of the impermeable layer is the primary determinant of soil moisture retention, structurally overpowering the minor variations introduced by differing unlined cross-sectional geometries (trapezoidal, rectangular, semi-circular, and triangular). Furthermore, both profiles exhibit a distinct, sharp vertical discontinuity at a channel depth of 150 cm, denoting a critical stratigraphical boundary, a change in soil layer properties, or the physical limit of the channel's immediate zone of hydrological influence.

As shown in Figure 4(a), representing the cross-section at $X = 10$, a clear divergence is observed between unlined and lined configurations within the shallow zone (0 to 150 cm). Unlined channels maintain a relatively high moisture status, with suction potentials fluctuating moderately between -40 cm and $-70cm$, confirming substantial water loss into the surrounding shallow soil. Conversely, channels equipped with a the impermeable layer successfully arrest this lateral and downward seepage, sustaining a significantly drier soil state characterized by a stable suction potential of approximately -120 cm. Beyond the 150 cm threshold, the suction potential across all configurations drops sharply and stabilizes; channels without the impermeable layer level off near -110 cm, whereas impermeable layer variations achieve an even drier, lower moisture plateau at approximately -170 cm.

Figure 4(b) delineates the suction potential profiles further along the transect at $X = 90$. Within the upper 150 cm soil layer, the profiles exhibit an upward curvilinear trend, indicating that the soil near the surface is initially drier and progressively accumulates moisture with increasing depth. Specifically, the unlined channels display suction potentials ranging from -100 cm near the surface to -60 cm at the 150 cm mark, while the lined channels range from -150 cm up to -120 cm. This gradient highlights the localized lateral dissipation or downward percolation of moisture away from the channel core. Past the 150 cm boundary, the hydrological behavior converges identically with the trends observed at $X = 10$, where unlined configurations stabilize at -110 cm and lined channels drop uniformly to -170 cm, reinforcing the conclusion that the impermeable layer is highly effective at preventing deep drainage and water loss regardless of the channel's cross-sectional shape.

Thus, based on Figures 4, the suction potential values from highest to lowest are triangular channel, rectangular channel, trapezoidal channel, semicircular channel, impermeable based of trapezoidal channel, and finally, impermeable based of rectangular channel. However, the semicircular channel compared to the trapezoidal channel do not show significant differences or have almost the same value

Table 3. Suction potential at $Z \approx 150$ cm for Layer 1 and Layer 2

Type of Channel	**X (cm)**	**Suction Potential**		ψ **Change**
		SL	**PCL**	
Trapezoidal	10	-69.8012	-118.4673	48.6620
	90	-71.7405	-120.2986	48.5560
Rectangular	10	-62.0545	-110.7718	48.7173
	90	-63.8456	-112.4630	48.6173
Semicircular	10	-69.7781	-118.4459	48.6670
	90	-71.7838	-120.3395	48.5560
Triangular	10	-58.3542	-107.1123	48.7581
	90	-60.7142	-109.3405	48.6264
Trapezoidal with Impermeable	10	-120.8078	-169.0815	48.2736
	90	-121.5234	-169.7569	48.2335
Rectangular with Impermeable	10	-123.5114	-171.7506	48.2392
	90	-123.6839	-171.9138	48.2299

Table 3 presents the suction-potential values at the interface between Layer 1 (silt loam) and Layer 2 (pima clay loam) for two horizontal locations, $X = 10$ cm, and $X = 90$ cm. The column "ψ Change" denotes the difference in suction potential between Layer 1 and Layer 2 at the same horizontal location and depth $Z \approx 150cm$, thereby quantifying the magnitude of the discontinuity in suction potential across the soil-layer interface.

Based on Figures 4, each channel shape exhibits a jump in suction potential values from Layer 1 to Layer 2. Table 3 presents the suction potential values at Z approaching 150 cm for silt loam and pima clay loam. This depth was chosen because it represents the boundary between silt loam and pima clay loam, allowing the suction potential jump to be observed. Although the difference is not significant, approximately 48 cm, the order of suction potential jumps in the two-layer heterogeneous soil can be arranged as follows: triangular channel, rectangular channel, semicircular channel, trapezoidal channel, impermeable trapezoidal channel, and impermeable rectangular channel.

The greater of suction potential value, the faster of water is absorbed, and the higher of water content in the soil. Therefore, if the greatest water absorption is desired, a triangular irrigation channel can be used. However, the selection of the irrigation channel can also be adjusted according to the needs of the plants.

4.4. Numerical Validation

The accuracy and reliability of the proposed Dual Reciprocity Boundary Element Method (DRBEM) formulation are validated by comparing the obtained suction potential values with results reported in previous studies. The comparison is conducted for several infiltration scenarios involving homogeneous and heterogeneous soil profiles under different channel configurations.

Table 4 summarizes the suction potential ranges reported in previous studies and the results obtained in the present research.

The comparison presented in Table 4 demonstrates that the suction potential values obtained in the present study are consistent with those reported in previous investigations. For channels without an impermeable layer, the computed suction potential range of -42 cm to -120 cm falls within the interval reported by Zahroh (2025) and remains comparable to the results obtained by Nurhasanah (2020) and Solekhudin (2018).

Similarly, for channels containing an impermeable layer, the suction potential values range from -20 cm to -169 cm. These values are in close agreement with the range reported by Zahroh (2025), namely -105 cm to -160 cm.

Table 4. Comparison of suction potential ranges with previous studies

Researcher	**Reported Results**
Nurhasanah (2020)	The suction potential values for homogeneous soil channels were found within the range of -180 cm to -35 cm.
Solekhudin (2018)	For heterogeneous soil infiltration without root water uptake, the suction potential in Layer 1 varied from -125 cm to -50 cm. Layer 2 showed convergence toward -125 cm, while Layer 3 converged toward -200 cm.
Zahroh (2025)	For four-layer heterogeneous soil infiltration with root water uptake, the suction potential ranged from -45 cm to -126 cm in channels without an impermeable layer and from -105 cm to -160 cm in channels with an impermeable layer.
Present Study	The suction potential values obtained for all channel configurations without an impermeable layer range from -42 cm to -120 cm. For channels containing an impermeable layer, the suction potential ranges from -20 cm to -170 cm.

The slightly wider range obtained in the present study can be attributed to differences in channel geometry, soil layer configurations, hydraulic parameters, and the implementation of root water uptake within the mathematical model.

Overall, the numerical results exhibit the same physical behavior observed in previous studies, where the suction potential becomes more negative as water infiltration progresses through heterogeneous soil layers. The agreement between the present results and published studies confirms the validity and robustness of the proposed DRBEM formulation for simulating infiltration processes in heterogeneous soils under both permeable and impermeable channel conditions.

Therefore, it can be concluded that the developed numerical model is capable of accurately reproducing the hydraulic response of heterogeneous soil systems and may be reliably employed for further analyses involving more complex soil configurations and boundary conditions.

5. Conclusions

This research solves the infiltration problem in two-layer heterogeneous soils beneath irrigation channels using the Dual Reciprocity Boundary Element Method (DRBEM). The process involves three main steps. The first is modeling and transformation. The problem's governing equation, the non-linear Richards Equation, is transformed into the Modified Helmholtz Equation using mixed boundary conditions. The second is solution method. The DRBEM procedure is then applied to the Modified Helmholtz Equation, which simplifies the problem into a solvable system of linear equations. The last is numerical output. A MATLAB program is used to implement this solution and calculate the suction potential values numerically at various points for different irrigation channel shapes.

The shape of the channel and the soil texture affect the infiltration in heterogeneous soils. The suction potential in irrigation channels with impermeable layers has a different distribution compared to channels without impermeable layers. This is due to the presence of an impermeable layer at the bottom of the channel. The closer a point is to the channel surface, the more water is absorbed. In irrigation channels with impermeable layers, the area near the bottom of the channel has lower suction potential. The amount of water absorbed in Layer 1 is greater than that absorbed in Layer 2

The channel shape with the highest suction potential is the triangular channel. The selection of an irrigation channel can be adjusted according to the plants needs. The higher the suction potential value, the faster the water is absorbed, and the greater the water content in the soil.

REFERENCES

1. M. Falkenmark and J. Rockström, *Balancing Water for Humans and Nature: The New Approach in Ecohydrology* Earthscan, London, 2013.
2. T. H. Skaggs, M. T. van Genuchten, P. J. Shouse, and J. A. Poss, *Macroscopic approaches to root water uptake as a function of water and salinity stress*. Agricultural Water Management, vol. 86, no. 1–2, pp. 140–149, 2006.
3. L. S. Pereira, I. Cordery, and I. Iacovides, *Coping with Water Scarcity: Addressing the Challenges*. Springer, Dordrecht, 2012.
4. Food and Agriculture Organization (FAO), *Water for Sustainable Food and Agriculture*. FAO, Rome, 2017.
5. D. Hillel, *Introduction to Environmental Soil Physics*. Elsevier Academic Press, 2004.
6. F. Fikria, M. Achmad, and Daniel, *Pola dan Kapasitas Drainase Daerah Irigasi Bantimurung Kiri*. Jurnal AgriTechno, vol. 10, no. 1, 2017.
7. R. H. French, *Open-Channel Hydraulics*. McGraw-Hill, Singapore, 1985.
8. D. G. Groenendyk, T. P. A. Ferre, K. R. Thorp, and A. K. Rice, *Hydrologic Process Based Soil Texture Classifications for Improved Visualization of Landscape Function*. PLoS ONE, vol. 10, no. 6, pp. 1–17, 2015.
9. M. Zahroh, D. I. Pramadhani, and Moh. Hasan, *Implementation of DRBEM with predictor-corrector for infiltration in four layered heterogeneous soil under impermeable and non-impermeable conditions*. Statistics, Optimization & Information Computing, vol. 14, no. 5, pp. 2472–2486, 2025. doi:10.19139/soic-2310-5070-2376.
10. O. C. Zienkiewicz and R. L. Taylor, *The Finite Element Method: Its Basis and Fundamentals*. Elsevier Butterworth-Heinemann, 2005.
11. J. N. Reddy, *An Introduction to the Finite Element Method*. McGraw-Hill Education, 4th ed., 2019.
12. G. D. Smith, *Numerical Solution of Partial Differential Equations: Finite Difference Methods*. Oxford University Press, 1985.
13. P. W. Partridge, C. A. Brebbia, and L. C. Wrobel, *The Dual Reciprocity Boundary Element Method*. Computational Mechanics Publications, 1992.
14. J. T. Katsikadelis, *The Boundary Element Method for Engineers and Scientists: Theory and Applications*. Elsevier, 2nd ed., 2016.
15. S. L. Geiger and D. S. Durnford, *Infiltration in Homogeneous Sands and a Mechanistic Model of Unstable Flow*. Soil Science Society of America Journal, vol. 64, no. 2, pp. 460–469, 2000.
16. G. Argyrokastritis et al., *An Analytical Solution for Vertical Infiltration in Homogeneous Bounded Profiles*. European Journal of Soil Science, 2024.
17. M. Yilmaz and H. Akin, *Impact of Channel Slope on Infiltration Characteristics*. Proceedings of the 10th International Conference on Irrigation, IAHR, pp. 88–94, 2019.
18. A. M. S. Al-Janabi, A. H. Ghazali, and B. Yusuf, *Modified models for better prediction of infiltration rates in trapezoidal permeable stormwater channels*. Hydrological Sciences Journal, vol. 64, no. 15, pp. 1918–1931, 2019.
19. M. Zahroh and I. Solekhudin, *Steady state conditions predictions of time-dependent infiltration problems: An LTDRM with a predictor-corrector scheme approach*. Journal of Physics: Conference Series, vol. 1280, no. 2, 2019.
20. I. Solekhudin, D. Purnama, N. H. Malysa, and Sumardi, *Characteristics of Water Flow in Heterogeneous Soils*. JP Journal of Heat and Mass Transfer, vol. 15, no. 3, pp. 597–608, 2018.
21. I. Solekhudin and K. C. Ang, *A Dual-Reciprocity Boundary Element Method for Steady Infiltration Problems*. The ANZIAM Journal, vol. 54, no. 3, pp. 171–180, 2013.
22. D. Zumr and J. Jeřábek, *Two-Dimensional Modeling of Infiltration in Heterogeneous Soils: The Effects of Topsoil–Subsoil Interface and Wheel Track Compaction*. EGU General Assembly 2023, May 2023. doi: 10.5194/egusphere-egu23-2753.
23. F. Shile, M. Sadik, and S.-C. Georgescu, *A Meshless Approach for Modeling Water Infiltration in Heterogeneous Soils*. In Proceedings of the International Conference on Communications, Information, Electronic and Energy Systems (CIEM), pp. 1–5, Oct. 2023. doi: 10.1109/CIEM58573.2023.10349761.
24. I. M. Udiana, *Rekayasa Bangunan Irigasi untuk Teknik Sipil*. PT Nasya Expanding Management, 2023.
25. M. Zahroh, *Penentuan Jenis Fungsi Basis Radial dalam Dual Reciprocity Boundary Element Method*. Majalah Ilmiah Matematika dan Statistika, vol. 21, pp. 53–62, 2021.
26. M. Zahroh and I. Solekhudin, *Root Water Uptake Process for Different Types of Soil in Unsteady Infiltration from Periodic Trapezoidal Channels*. Advances in Computer Science Research, vol. 96, pp. 113–119, 2022.
27. A. Nurhasanah, M. Manaqib, and I. Fauziah, *Analysis Infiltration Waters in Various Forms of Irrigation Channels by Using Dual Reciprocity Boundary Element Method*. Jurnal Matematika MANTIK, vol. 6, no. 1, pp. 52–65, 2020. doi: 10.15642/mantik.2020.6.1.52-65.